Proceedings of the ASME 2010 Conference on Smart Materials, Adaptive Structures and Intelligent Systems
SMASIS2010
September 28 - October 1, 2010, Philadelphia, Pennsylvania, USA

SMASIS2010-3852

METAL-MATRIX COMPOSITE METAMATERIALS WITH SMART SWITCHES EMBEDDED BY ULTRASONIC CONSOLIDATION

C.D. Hopkins[*]
D. Foster[†]
M.J. Dapino[‡]
Smart Materials and Structures Laboratory
Department of Mechanical Engineering
The Ohio State University
Columbus, Ohio 43210
Email: dapino.1@osu.edu

L. Zhang

Electro-Science Laboratory
Department of Electrical and Computer Engineering
The Ohio State University
Columbus, Ohio 43210
Email: zhang.471@osu.edu

ABSTRACT

This research deals with the development of metal-matrix composite metamaterials with embedded electrical switches made of shape memory nickel-titanium (Ni-Ti) for use in broadband radio frequency (RF) antennas. We have created an experiment that illustrates how a Ni-Ti ribbon can form an electrical contact that opens and closes depending on the Ni-Ti phase being austenite or martensite. We have conducted finite element analyses that describe the thermal gradients in the ribbon required for effecting the phase change. Since part of the embedded Ni-Ti has to be electrically insulated from the aluminum matrix, we have investigated various insulation techniques and selected one that is both effective and straightforward to implement. In order to realize multiband/broadband metamaterials, it is necessary to seamlessly embed the Ni-Ti switches into the metamaterial for active reconfiguration of the electromagnetic response. To achieve this reconfiguration we utilize ultrasonic consolidation (UC), a new manufacturing technology that uses solid state ultrasonic metal welding (UMW) to create metal parts at relatively low temperatures. Consideration of the proposed RF switch for load-carrying antennas requires an aluminum matrix with structural-grade strength; we have conducted mechanical testing which quantifies the longitudinal tensile, transverse tensile, and shear strength of the UC matrix. Preliminary tests have been completed to evaluate the performance of an antenna device with integrated Ni-Ti switch.

Keywords: Ultrasonic consolidation, metamaterials, metal matrix composites, smart materials, RF antennas.

INTRODUCTION

Metamaterials are manmade, three-dimensional periodic cellular architectures designed to exhibit optimized responses. Much attention has been given in recent years to metamaterials for radio frequency and optical applications. However, these materials are intrinsically narrowband and hence their use has been limited to narrowband ground planes to emulate magnetic layers or realize thinner conformal antennas [1–3].

The overarching objective of this research is to create the science for overcoming the narrowband limitation of metamaterials and realizing multiband/broadband structural antennas with potential frequency bandwidth of 30:1 (100-3000 MHz). Specifically, smart materials are used to design the antenna metallization with reconfiguration through mechanical and electromechanical tuning. Example applications include the ability to realize miniature conformal ultra wideband antennas (30 to 3000 MHz) on

[*]Email: hopkins.626@osu.edu
[†]Email: foster.373@osu.edu
[‡]Address all correspondence to this author.

thin and flexible substrates for small Unmanned Aerial Vehicles (UAVs), high gain antennas for portable devices enabling high data rate communications via ground and satellite means, and multifunctional and reconfigurable apertures.

This paper presents the design and fabrication of metal-matrix composites with embedded reconfiguration based on smart materials such as Ni-Ti shape memory alloys (SMAs). Shape memory alloys possess the ability to be plastically deformed and then recover their original shape when the temperature is increased above the material's austenitic finish temperature. Ni-Ti is a specific type of SMA that is able to be strained up to 8% and fully recover all deformation [4]. The ability of Ni-Ti to have such large strains be recoverable is due to the crystalline structure of the alloy transforming between the martensitic and austenitic phases [5]. The research presented herein takes advantage of this unique characteristic of Ni-Ti by using it as a solid state actuator to open and close a simple electrical switch or tunable phase shifter.

The manufacturing process utilized to seamlessly embed smart materials into metal matrices is ultrasonic consolidation (UC), also known as ultrasonic additive manufacturing (UAM). UAM is a recent manufacturing process that combines principles from ultrasonic metal welding (UMW), layered manufacturing techniques, and subtractive processes to create metal parts with arbitrary shapes and features [6]. UAM is a solid-state welding process that allows joining of metallic materials far below their respective melting temperatures. The locally generated heat due to ultrasonic vibration during the UAM process ranges between 30%-50% of the melting temperature of the base metal [7]. Being a relatively low-temperature process, UAM offers unprecedented opportunities to create parts with embedded smart materials or electronic components [8, 9]. Further, the subtractive stage integrated within the UAM system allows for the simultaneous incorporation of arbitrarily shaped internal features such as cooling channels or designed anisotropies.

A sonotrode or horn is used to apply a normal force at the interface between two metal work pieces. Ultrasonic transducers drive the transversely vibrating sonotrode which imparts a motion to the top work piece and creates a relative, friction-like action at the interface of the two work pieces. This scrubbing motion causes shear deformations of contacting surface asperities, dispersing interface oxides and ultimately bringing clean metal-to-metal contact and adhesion between the faying surfaces [10]. A diagram of the UAM process is seen in Fig. 1.

The UAM system is distinct from conventional metal welding systems; it consists of a rotating transducer, booster, and horn arrangement. As shown in Fig. 2, vibrations generated by a piezoelectric ultrasonic transducer are transmitted into the parts through a rolling sonotrode. The vibrations propagate longitudinally at a frequency of 20 kHz from the transducer to the sonotrode through tuned waveguides. The amplitude of vibration is considered a process parameter that can be adjusted. Normal

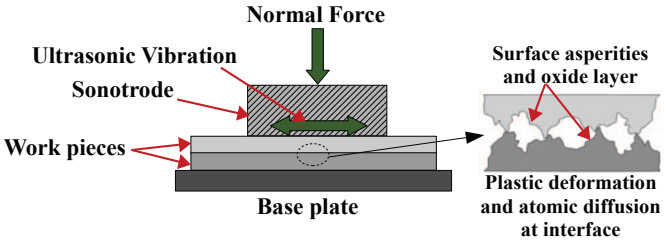

FIGURE 1. SCHEMATIC REPRESENTATION OF ULTRASONIC CONSOLIDATION AT THE INTERFACE BETWEEN TWO METAL SURFACES.

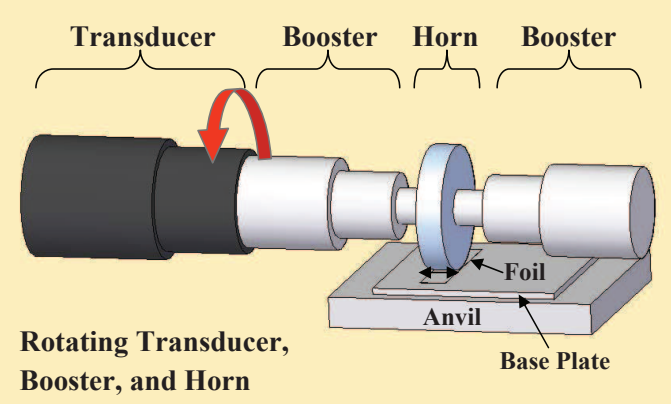

FIGURE 2. DIAGRAM OF UAM SYSTEM WHERE SUCCESSIVE LAYERS OF METAL TAPE ARE BONDED TOGETHER FOR CREATING BULK METALLIC PARTS.

force can be adjusted and is applied to the vibrating sonotrode as it rolls along the work piece. Current UAM systems achieve the most effective bonding on thin metal layers of approximately 152 μm thickness. The UAM system therefore employs an automated feed mechanism for allowing successive layers of metal tapes, drawn from a continuous spool, or thin sheets to be bonded together for creating larger bulk builds. In this research, UAM is utilized to embed shape memory Ni-Ti features that open and close electrical connections when energized.

DEVELOPMENT OF SMA SWITCH

Geometry and Proof of Concept

In order to keep the switch mechanism as simple as possible while still performing the required action, several switch configurations were considered. The main constraints and considerations surrounding the creation of the switch include the size of the gap needed to prevent electrical arcing at the switch contact point, the geometry and material needed to close the switch, the geometry and material needed to open the switch, and the method

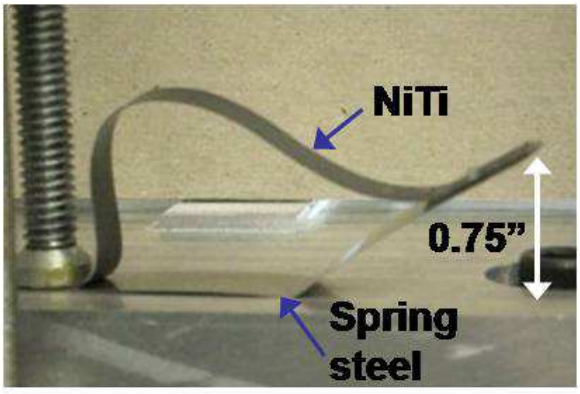

FIGURE 3. NORMALLY OPEN NI-TI AND STEEL SWITCH CONFIGURATION AND GEOMETRY.

FIGURE 4. 0.102 MM THICK NI-TI STRIP ELECTRICALLY INSULATED BY KAPTON FILM AND EMBEDDED BY UAM INTO ALUMINUM MATRIX.

and material for joining parts of the switch. Study of various geometries and materials showed that a normally open switch could be most easily configured, tested, and embedded by UAM into a metal matrix as a first pass. A bilayer of 7.62 mm wide by 0.254 mm thick Ni-Ti strip and 12.7 mm wide by 0.102 mm thick spring steel was found to work best after experimenting with pieces of varying thickness steel. The final configuration of steel and Ni-Ti can be seen in Fig. 3.

In this configuration, the Ni-Ti ribbon pushes down on the spring steel as it attempts to restore its flat memorized shape during the martensite to austenite transformation. Once heating ceases, the Ni-Ti plastically deforms back up due to the elasticity of the spring steel. Assisted by the kinematic gain created by the bump in the Ni-Ti ribbon, the total travel of the switch was 1.905 cm, and was later reduced to about 0.50 cm. This allows for a shorter switching time and reduced overall size which is beneficial for embedment. A configuration has been created for a normally closed switch with testing and geometry optimization ongoing.

Electrical Insulation

Electrically insulating the Ni-Ti and spring steel bilayers from the surrounding metal matrix and from each other is critical to the operation of the switch. The insulation ensures that electrical contact is achieved only when the shape memory ribbon is actuated. The insulation needs to be joined to the Ni-Ti ribbon, which has been found to be difficult in the past. Further, it is desired that the insulation layer be as thin as possible so as not to disrupt the embedding process. Finally, it needs to be tough enough to withstand the high oscillatory shear forces present during the UAM process.

We have investigated several different methods and materials for electrically insulating the Ni-Ti and spring steel bilayers. Two of them were insulation coatings including Epoxylite insul-spray clear enamel, and a polyimide based insulating varnish. It was found that, while both coatings were able to fully encapsulate and insulate the Ni-Ti, neither was able to withstand the embedding process. Post-embedding tests found that there was electrical conductivity between the Ni-Ti and the surrounding aluminum matrix. A Teflon coating was also applied to the Ni-Ti piece, but the layer applied was not thick enough to fully insulate the strip. This option was not further pursued. Another option was to anodize the Ni-Ti in order for a thick oxide layer to form on the surface of the strip. Numerous attempts were unsuccessful at producing a thick enough layer to fully encapsulate the Ni-Ti strip. Finally, Kapton film was shown to be an effective insulator (Fig. 4). It electrically insulates the steel and Ni-Ti, and it is thin enough (0.127 mm) as to not hinder embedding. In this research we showed, for the first time, that Kapton can withstand the oscillating shear forces created during the UAM process. Epoxy is used to adhere the Ni-Ti ribbon to the spring steel at the tip.

Switch Design and Finite Element Modeling

Photographs of the switch actuation cycle with an externally applied heat source are shown in Fig. 5. The Ni-Ti ribbon was machined via electron discharge machining (EDM) so that there is a small gap in the strip through part of its length as illustrated in Fig. 6. This allows for an electric circuit to be created such that current passed through the Ni-Ti ribbon creates ohmic heating and an associated phase transformation.

The antenna setup thus consists of a high current circuit for heating of the Ni-Ti ribbon and a low current switchable circuit that creates the test signal. Figure 7 shows a diagram of the setup used for testing the switch. The Ni-Ti ribbon and most of the spring steel are fully encapsulated in Kapton film. A small portion of the spring steel at the tip was left un-insulated in order for

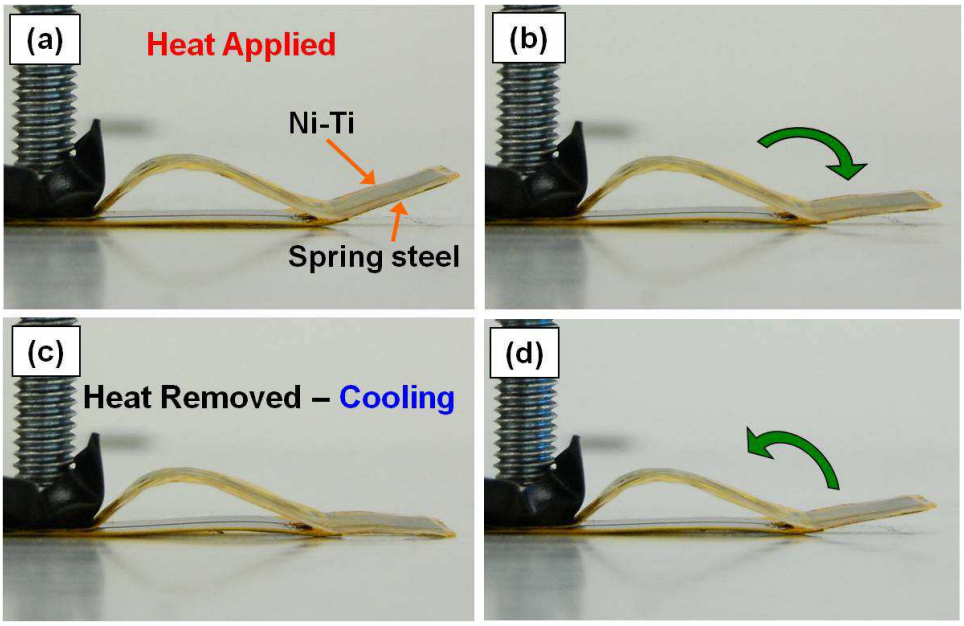

FIGURE 5. PHOTOGRAPHS OF SMA SWITCH WHERE (a) SWITCH IS IN INITIAL POSITION; (b) HEATING HAS BEGUN AND SWITCH BEGINS TO CLOSE; (c) SWITCH HAS FULLY CLOSED AND IS IN CONTACT WITH METAL BELOW; (d) COOLING HAS BEGUN AND SWITCH RETURNS TO ORIGINAL POSITION UNDER THE ACTION OF THE SPRING STEEL.

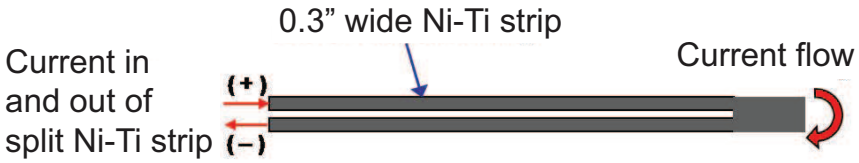

FIGURE 6. SCHEMATIC OF NI-TI STRIP CIRCUIT USED FOR RESISTIVELY HEATING THE SMART SWITCH.

current to run through the switch to the metal matrix surrounding it. Behind the bump portion of the Ni-Ti the bilayer was mechanically clamped in order to prevent the Ni-Ti from actuating in the wrong direction as well as to simulate the conditions that would occur when embedded.

One power supply produces a DC current of about 5 A which is directed through the Ni-Ti strip circuit to resistively heat the Ni-Ti ribbon. The second power supply is used to create the test signal. When the switch is open there is no current running through the steel and aluminum matrix circuit. When the switch is fully closed a current flows through the steel (at the exposed end) into the aluminum and back to the power supply (test signal). During testing, the currents were measured simultaneously; the resulting current versus time plot is shown in Fig. 8.

Figure 8 shows the current being ramped up to the desired value of about 5 A and holding while the Ni-Ti austenitic phase transformation temperature is being reached and the switch is beginning to actuate (0 - 17 seconds). The switch is then fully closed and the test signal (blue-dashed line) steps up to a current of about 0.75 A and holds (17 - 27 seconds). The current through the Ni-Ti is then shut-off and the switch begins to cool until it breaks contact and the test signal is cut (27 - 36 seconds). This test proves that the switch works correctly. The actuation speed can be optimized depending upon the current applied through the Ni-Ti, the distance that the switch needs to travel in order to make contact, and the cooling conditions.

Finite element analysis using Comsol Multiphysics 3.5a was performed on the Ni-Ti switch geometry to simulate heating and cooling cycles during operation. A Ni-Ti ribbon with a 4.06 cm mechanically free section (actuating portion) and a 16.26 cm section encapsulated in an aluminum matrix, was modeled. A 4.95 A current was used to heat the wire by conducting the current through the right side of the split end of the Ni-Ti with the left side of the split end being grounded.

Finite element analysis of the Ni-Ti model shows that the section of Ni-Ti encapsulated in the aluminum matrix rises only

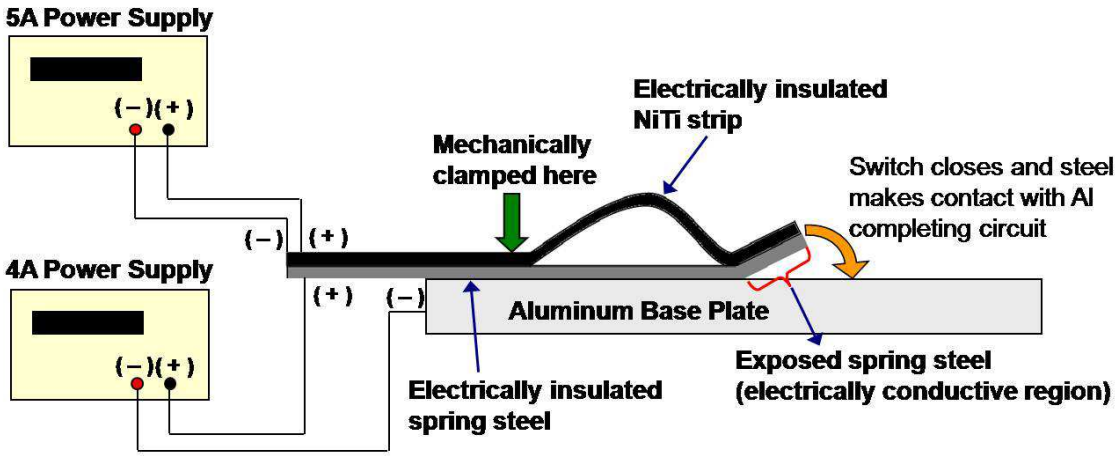

FIGURE 7. DIAGRAM OF SET-UP USED FOR TESTING THE SMA SWITCH.

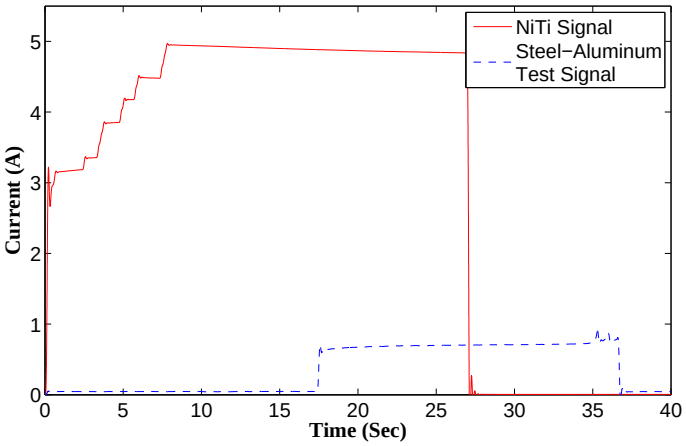

FIGURE 8. PLOT OF CURRENT VS TIME SHOWING THE CLOSING OF THE SMA SWITCH, RESULTING CURRENT THROUGH THE STEEL-ALUMINUM CIRCUIT, OPENING OF THE SMA SWITCH, AND TIME DELAYED RESPONSE OF OPENING OF STEEL-ALUMINUM CIRCUIT.

1°C while the mechanically free section of the Ni-Ti increases to much higher temperatures (Fig. 9). Temperature as a function of time plots for the three main section examined are shown in Fig. 10. The split portion of the mechanically free section of the Ni-Ti actuator increases to a peak temperature of 70°C at the applied current. The mechanically-free large cross-section at the tip experiences lower temperatures than the split portion of the Ni-Ti ribbon because of lower electrical power created due to its larger cross sectional area as well as less current flowing through the segment because of its greater impedance. This variation in temperature in the actuating region indicates that during resistive heating only the split portion in the actuation region transforms to austenite and applies a force on the cantilever spring to complete the circuit. The larger tip region remains in the martensite phase during the entire thermal cycle and serves only as a physical connection between the cantilever spring and the switch. Thus, the Ni-Ti geometry used maximizes the efficiency of the switch by only using enough current to sufficiently heat the small section that applies the force (split section) while not wasting current on sections that do not contribute to the actuation. The cooling cycle of the Ni-Ti switch occurs relatively fast due to the aluminum matrix conducting the heat out of the Ni-Ti ribbon more rapidly than if the ribbon were in ambient air only as shown in Fig. 11.

UAM COMPOSITES AND SWITCH INTEGRATION

Mechanical Characterization of UAM Matrix

The mechanical properties of UAM-fabricated parts govern the range of applications for which the process may be used. With traditional isotropic materials, the properties of primary importance are the tensile strength and shear strength of the given material. Due to the anisotropic nature of UAM fabricated materials, the strengths are multi-directional properties. Three distinct UAM samples (Fig. 12) were made to test the strength of the UAM matrix in shear, transverse tensile, and longitudinal tensile loading conditions. The averaged results of the mechanical tests are shown in Table 1. It has been found that shear and transverse tensile samples fail in a sudden, macro-brittle fracture mode and have strengths less than that of the parent material. Longitudinal tensile samples exhibit ductile failure in addition to an increase in strength over that of the parent material. It has been suggested that the increased strength is due to grain refinement from the horn texture and ultrasonic vibration [11]. It has also been found

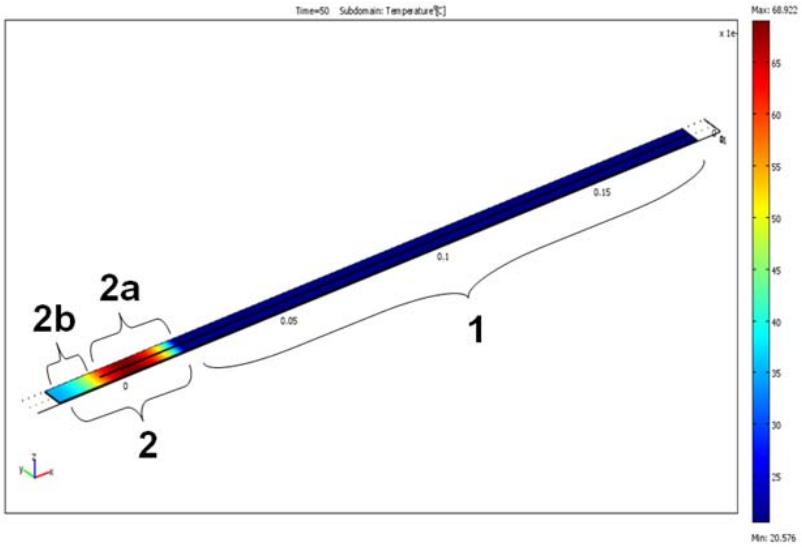

FIGURE 9. MODELED TEMPERATURE PROFILE OF NI-TI ACTUATOR AFTER 50 SECONDS OF HEATING WHERE REGION 1 IS NI-TI IN AL MATRIX; REGION 2 IS THE MECHANICALLY FREE SEGMENT; REGION 2a IS THE ACTUATING SPLIT SECTION; REGION 2b IS THE TIP CONTACT AREA.

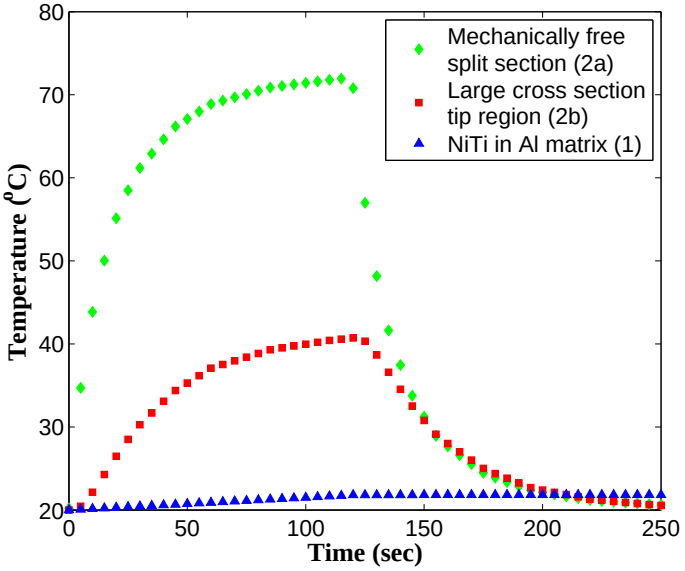

FIGURE 10. TEMPERATURE VS TIME PLOT OF DIFFERENT SECTIONS OF NI-TI SWITCH.

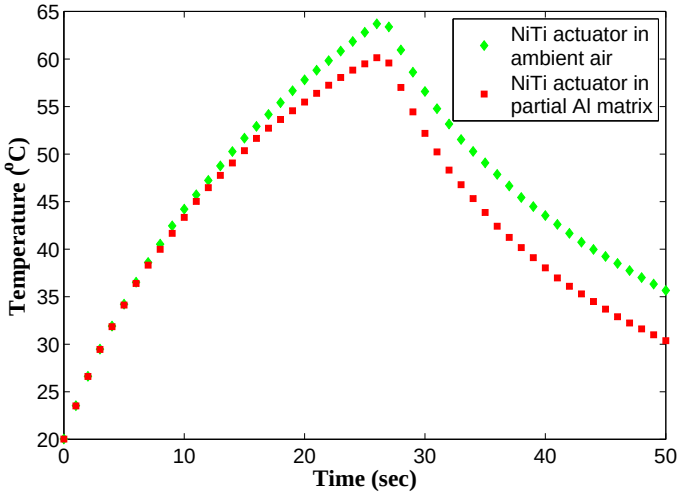

FIGURE 11. TEMPERATURE VS TIME PLOT OF NI-TI IN AMBIENT AIR COMPARED TO NI-TI PARTIALLY EMBEDDED IN AL MATRIX.

that the strength of the UAM builds is significantly influenced by the machine setting conditions and much research has been devoted to determining the optimal levels of the process parameters in order to maximize the mechanical strength of UAM specimens [7, 12, 13]. Overall, the results of these mechanical tests indicate that orientation of UAM structures relative to loading conditions is critical.

Embedding of Switch into UAM Matrix

The switch was successfully embedded using Edison Welding Institute's (EWI) VHP-UAM Test Bed with a 4450 N nor-

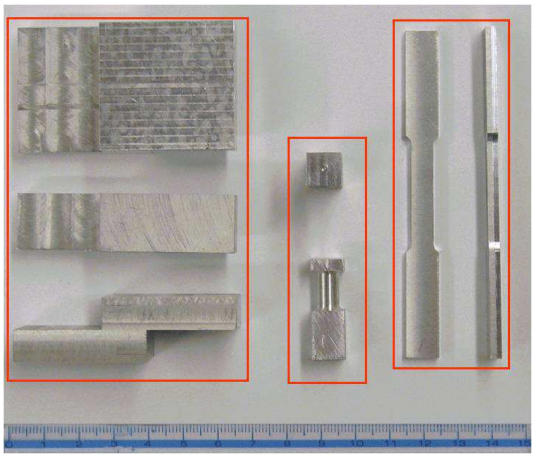

FIGURE 12. PHOTOGRAPH OF UAM MECHANICAL STRENGTH TEST SAMPLES - (LEFT TO RIGHT) TRANSVERSE SHEAR SAMPLES, TRANSVERSE TENSILE SAMPLES, LONGITUDINAL TENSILE SAMPLES.

mal force, 31.2 μm oscillation amplitude, and 25.4 mm/sec weld rate. The switch was embedded into a metallic matrix composed of 3003 H-18 aluminum using UAM. The switch is flipped over such that it closes upward making contact with the aluminum tape above it. It has been previously shown that designed internal features can be machined during the build process in the UAM Beta system [10], but for simplicity the pocket and groove were machined out of solid 3003 aluminum and four layers were laid over top by UAM. Figure 13 shows a three-dimensional CAD model of the switch and matrix geometry to be used for embedding with a photograph of the actual piece prior to embedment. Figure 14 is a photograph of the embedded switch.

RF STUDY

Experimental Set-up

A simple quarter wavelength ($\lambda/4$) monopole antenna was designed and fabricated to evaluate the effect from the Ni-Ti switch on the antenna performance. As shown in Fig. 15, the aluminum monopole is 25.4 cm tall and 0.457 cm in diameter, centered on a 81.28 cm diameter aluminum ground plane. These dimensions are chosen so that the antenna effectively works at ~300 MHz [15]. The switch was located close to the monopole and supported by Styrofoam™(the foam does not interfere with the electromagnetic signals or the antenna performance). The split end of the switch was connected to a DC power supply (Agilent E3631A). Two ferrite chokes were used on the connecting wires to isolate the RF signals from the DC current because the wire and connections are within the near-field region (~1 m radius) for this particular set-up and thus can become coupled to the antenna system. When no current was applied ("switch off"), there was no contact between the monopole and the switch. When the current was applied ("switch on"), the switch bent and eventually touched the top of the monopole. In other words, this antenna has a straight monopole in the "switch off" state, and a reconfigured bent monopole in the "switch on" state. The RF signals were delivered from the bottom of the monopole and the return loss was measured by a network analyzer (Agilent N5242A, PNA-X) as it swept through a range of frequencies. The return loss is a dB scaling of the antenna parameter, reflection coefficient S_{11}, which is given by [16]

$$S_{11} = \frac{V_r}{V_i} \tag{1}$$

where V_r and V_i are the reflected and incident voltages, respectively. The return loss as measured by the network analyzer is given by [16]

$$RL = 20log_{10}|S_{11}|. \tag{2}$$

This can also be written in terms of a power ratio such that $(V_r/V_i)^2 = (P_r/P_i)$ where P_r and P_i are the reflected and incident powers, respectively. In this case the return loss would be

$$RL = 10log_{10}\left|\frac{P_r}{P_i}\right|. \tag{3}$$

Since S_{11} is determined by the antenna geometry and related impedance, it is useful for evaluating the performance changes at the different on and off switch states. The more negative S_{11} (in dB) is, the less a signal is reflected back, thereby increasing the signal transmitted which ultimately leads to better RF performance.

Results

As depicted in Fig. 16, the minimum S_{11} was -15.1 dB at 270 MHz when the switch is off. When energized, the switch gradually bent toward the monopole, while the resonance frequency was accordingly shifting to a lower frequency. Once the switch was in contact with the monopole, S_{11} was -14.5 dB at 185 MHz. The downward shift of the resonance peak is due to the extended length of the monopole in the "switch on" state. It is also noted that S_{11} was less than -10 dB in both of the "off" and "on" states. This means that the reflected power was less than 10%, which is satisfactory for a working antenna. Therefore, this simple measurement shows that the antenna reconfiguration can be achieved by incorporation of the Ni-Ti switch. In particular, the antenna RF performance was tuned by the geometry change of the switch resulting from the applied DC current.

TABLE 1. RESULTS OF UAM MECHANICAL STRENGTH TESTS AND COMPARISON TO BULK 3003 H-18 ALUMINUM.

Mechanical Strength	Al 3003 H-18 (MPa) [14]	UAM Sample (MPa)	Percent of Parent Material	Coefficient of Variance
Ultimate Shear	110	53	47.8%	16.6%
Ultimate Transverse Tensile	200	30	15.2%	9.45%
Ultimate Longitudinal Tensile	200	236	117.8%	2.46%

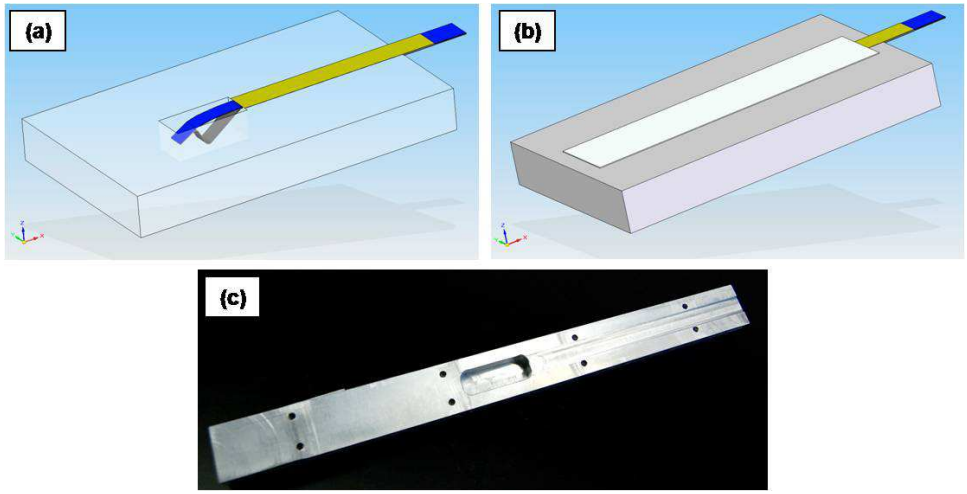

FIGURE 13. 3D CAD MODEL OF (a) NI-TI (BLACK) AND SPRING STEEL (BLUE) WRAPPED IN KAPTON (GOLD) IN CONFIGURATION TO BE EMBEDDED AND (b) RESULTING EMBEDDED SWITCH WITH ALUMINUM LAYER (WHITE) ON TOP. (c) PHOTOGRAPH OF MACHINED ALUMINUM PIECE PRIOR TO INSERTION OF SWITCH AND EMBEDDING.

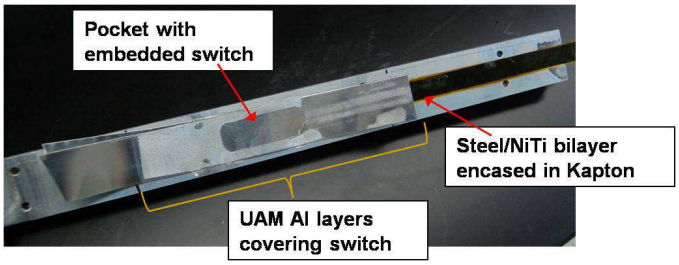

FIGURE 14. PHOTOGRAPH OF UAM EMBEDDED NI-TI SWITCH.

CONCLUSIONS AND FUTURE WORK

We have completed the initial steps towards creating a structural antenna made of a metal-matrix composite metamaterial with broadband reconfiguration. A proof-of-concept smart material (Ni-Ti) switch was successfully created. Kapton film was found to be a robust electrical insulator that could withstand the high shear forces that are present during UAM embedding. An experiment was devised and carried out to test the actuation properties of the switch. It was found that a steady test signal can be applied through the spring steel and aluminum matrix by running a separate high current through the Ni-Ti to resistively heat the switch and create the desired actuation. Finite element modeling showed that only the small region that provides the actuation is being heated which will allow for optimization of the switch geometry in the future. Mechanical tests including transverse shear, transverse tensile, and longitudinal tensile were conducted on 3003 aluminum UAM built samples and it was found that the orientation of the structure relative to the loading conditions is critical. Finally, RF performance tests using a simple monopole antenna and ground plane prove that a shift in resonant frequency of the antenna system is achievable through the actuation of the SMA switch.

In order to realize the ultimate goal of the project, several steps will be taken in the future. Firstly, switch miniaturization needs to be realized. The current switch is too large because it is desired that millimeter-size switches be embedded. We will then address any fabrication challenges and new heat transfer proper-

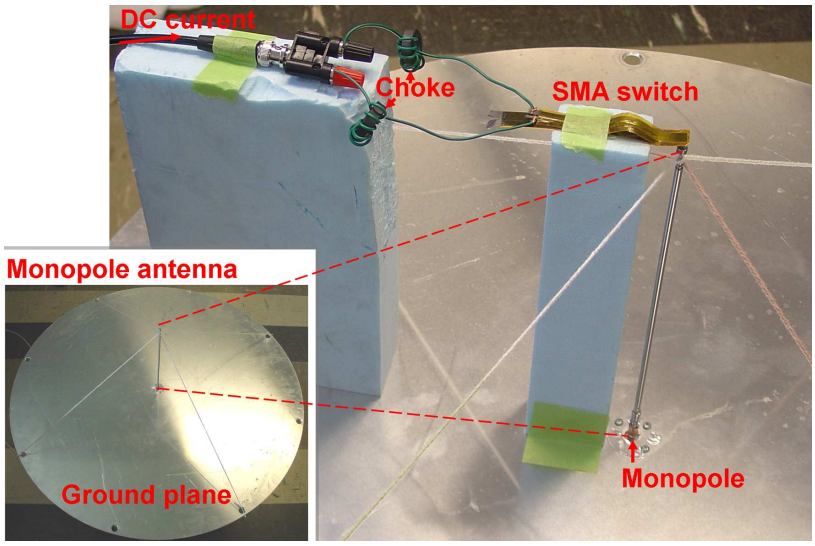

FIGURE 15. IMAGES OF MONOPOLE ANTENNA AND SHAPE MEMORY ALLOY (SMA) SWITCH SET-UP FOR RF PERFORMANCE TESTING.

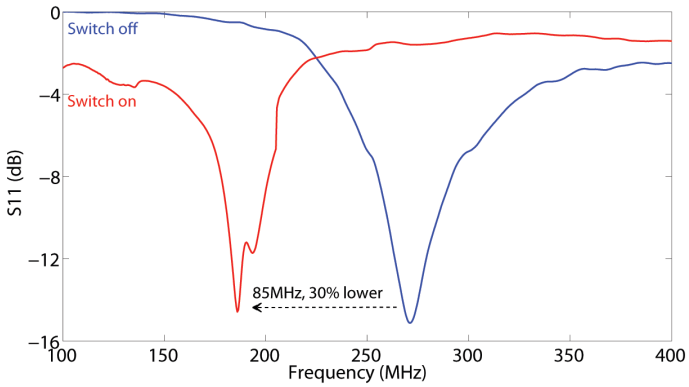

FIGURE 16. RETURN LOSS AS A FUNCTION OF FREQUENCY FOR SWITCH OFF AND SWITCH ON STATES.

ties of the mini-switches and augment the existing finite element models through fully coupled models for thermoelastic response. Secondly, we need to create a network of switch arrays and be able to demonstrate the fabrication of a simple array of switches as well as mechanically and electrically characterize the resulting networks. Thirdly, we will build upon our preliminary RF performance test results and develop design rules for complex antenna systems. Also, we will address the multiphysics responses relating electromagnetic, mechanical fatigue, and thermal issues caused by signal power. Finally, in order to design realizable and repeatable performance RF devices, a multiphysics numerical characterization will need to be adapted as well.

ACKNOWLEDGMENT

The authors would like to thank Dr. Karl Graff and Matt Short of Edison Welding Institute, Dr. John Volakis and Jing Zhao of the OSU Electro-Science Laboratory, and Ryan Hahnlen of the Mechanical Engineering Department. Financial support for this research was provided by the OSU Institute for Materials Research Interdisciplinary Materials Research Grant, the Ohio Space Grant Consortium, and the Smart Vehicle Concepts Center (www.SmartVehicleCenter.org), a National Science Foundation Industry/University Collaborative Research Center.

REFERENCES

[1] Volakis, J., Mumcu, G., Sertel, K., Chen, C., Lee, M., Kramer, B., Psychoudakis, D., and Kiziltas, G., 2006. "Antenna Miniaturization Using Magnetic-Photonic and Degenerate Band-Edge Crystals". *IEEE Antennas and Propagation Magazine*, ***48***(5), pp. 12–28.

[2] Caloz, C., 2009. "Perspectives on EM metamaterials". *Materials Today*, ***12***(3), pp. 12–20.

[3] Ziolkowski, R., 2008. "An Efficient, Electrically Small Antenna Designed for VHF and UHF Applications". *IEEE Antennas and Wireless Propagation Letters*, ***7***, pp. 217–220.

[4] SAES Smart Materials, 2009. Nitinol data. http://www.shape-memory-alloys.com

[5] Lagoudas, D., 2008. *Shape Memory Alloys*. Science and Business Media, LLC.

[6] Graff, K., 2005. *New Developments in Advanced Welding*. Woodhead Publishing Limited.

[7] Kong, C., Soar, R., and Dickens, P., 2004. "Optimum pro-

cess parameters for ultrasonic consolidation of 3003 aluminum". *J. of Materials Processing Tech.*, ***146***(2), pp. 181–187.

[8] Kong, C., and Soar, R., 2005. "Fabrication of metal–matrix composites and adaptive composites using ultrasonic consolidation process". *Materials Science & Engineering A*, ***412***(1-2), pp. 12–18.

[9] Siggard, E., 2007. "Investigative research into the structural embedding of electrical and mechanical systems using ultrasonic consolidation". Master's thesis, Utah State University, Logan, UT.

[10] White, D., 2003. "Ultrasonic consolidation of aluminum tooling". *Advanced materials & processes*, ***161***(1), pp. 64–65.

[11] Johnson, K., 2008. "Interlaminar subgrain refinement in ultrasonic consolidation". PhD thesis, Loughborough University, Loughborough, UK.

[12] Kulakov, M., and Rack, H., 2009. "Control of 3003-H18 Aluminum Ultrasonic Consolidation". *Journal of Engineering Materials and Technology*, ***131***, p. 021006.

[13] Janaki Ram, G., Yang, Y., and Stucker, B., 2006. "Effect of Process Parameters on Bond Formation During Ultrasonic Consolidation of Aluminum Alloy 3003". *Journal of Manufacturing Systems*, ***25***(3), p. 221.

[14] The Aluminum Association, 1979. *Aluminum Standards and Data*, 6th ed.

[15] Kraus, J., and Marhefka, R., 2003. *Antennas For All Applications*, 3rd ed. McGraw-Hill.

[16] Pozar, D., 1998. *Microwave Engineering*, 2nd ed. John Wiley & Sons.